Structural and Electromechanical insights into Thermoplastic Polyurethane/3D Hybrid Carbon Nanocomposites towards Strain Sensor Applications

Vaishnav. B[1,2], Benedikt Sochor[2,3], Ajay Gupta[1], Sarathlal Koyiloth Vayalil[2,1]*

[1]Department of Physics, Applied Science Cluster, UPES, Dehradun, 248007 India

[2]Deutsches Elektronen-Synchrotron DESY, Notkestrasse 85, 22607 Hamburg, Germany

[3]Advanced Light Source, Lawrence Berkeley National, Laboratory, 6 Cyclotron Rd, Berkeley, CA 94720, USA

**Corresponding author email: sarathlal.koyiloth.vayalil@desy.de*

Abstract

Incorporation of different dimensional carbon allotropes within elastomeric matrices has been established as an effective strategy to fabricate functional conductive polymer nanocomposites (PNC). In this work, a higher dimensional 3D hybrid carbon nanofillers - comprising the synergistically integrated multi-walled carbon nanotubes immobilized into few-layers graphene – were incorporated into thermoplastic polyurethane (TPU) matrix, to demonstrate its effectiveness as a strain sensor. The conductive films fabricated through a simple solution casting technique, in which the mechanical, electrical and strain sensing characteristics are studied in view of filler's distribution, structural confinement, and interfacial interactions. Analyses using wide-angle X-ray

scattering, Raman spectroscopy, and tensile testing, revealed a higher degree of filler reinforcement within TPU moieties, indicating the pronounced interfacial interactions. Further, the tensile modulus heightened significantly with filler loading above their percolation threshold (363% for 20wt% loading). The structural features of dispersed filler aggregates were explored through an iterative model fitting of the ultra-small angle X-ray scattering (USAXS) data, along with scanning electron microscopy (SEM). As a strain sensor, the films displayed a superior working-strain Gauge Factor (GF=123), with an exceptional stability under both unidirectional and cyclic strain. Further, a large strain GF of 601.5 was evidenced for the composites with higher 3D filler loading. The findings provide a fundamental understanding, alongside validating the potential of hybrid carbonaceous fillers for the fabrication of PNCs with futuristic applications.

Keywords

Flexible strain sensors, Polyurethane, 3D Hybrid fillers, Small-angle X-ray scattering, Electromechanical properties.

ToC graphic

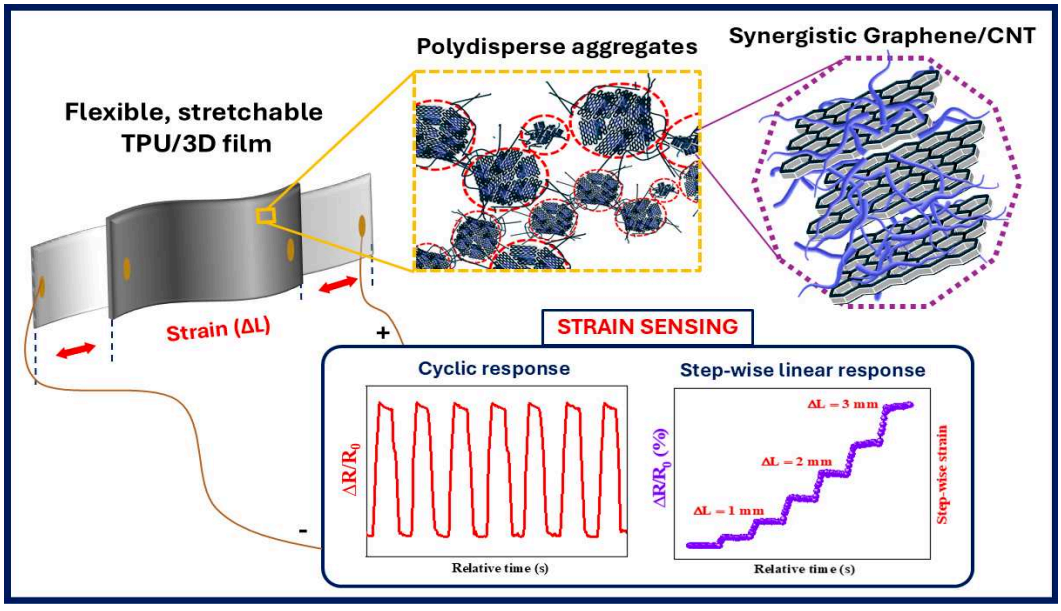

Introduction

Flexible, conductive elastomers are integral components in various applications, including wearable electronics [1–3], health monitoring [4–6], smart textiles [6–8], etc. The increasing demand for smart flexible materials has driven extensive research towards understanding, exploration and engineering of novel elastomeric materials. The innate properties of elastomers such as flexibility, softness, easier processability and tunability has been exploited to yield new materials with enhanced thermal[9,10], electrical[11–13], mechanical[9,14,15] properties, that showed heightened electromagnetic shielding[16,17], anti-microbial [18,19], corrosion resistance [20,21], energy storage [22–24], strain sensing behaviours [25–29]and so on. The resulting functionality of elastomer is decided by the nature of nanofillers being incorporated within them. Moreover, the concentration, distribution, and site-specific structure formation (aggregation) of nanofillers crucially decide the overall property of polymer nanocomposite (PNC).

Numerous studies on carbon-based PNCs revealed that carbon nanoparticles efficiently enhance the electrical conductivity, as well as mechanical and thermal stability of elastomers.[9,10,30] Allotropes such as carbon black (CB), carbon nanotube (CNT), graphene, possessing exceptional thermal and electrical conductivities (~10^3- 10^5 Sm^{-1}), high aspect ratios (1D and 2D nanoparticles), with huge intrinsic moduli (in case of graphene) are well-suited to meet the necessities. CNTs with high aspect ratios, introduced into both thermoplastic as well as thermosetting matrices has significantly reduced the electrical resistance. In the context of strain sensing behaviour, the sensitivity (quantified as Gauge Factor (GF)), large working strain and good cyclic stability were observed for CNTs. For example, Wang *et. al.* fabricated CNT/ polydimethylsiloxane (PDMS) sensor to obtain highly stretchable, sensitive strain sensor with tuneable sensitivity for human motion detection.[27] Park *et. al.* introduced MWCNTs in

polyethylene oxide (PEO), and reported a superior sensing behaviour than metal alloy strain gauges.[12] However, the moderate dispersion, limited extent of linear strain sensing serves as constraints. The infusion of graphene on the other hand has elevated the conductance, with increased linearity in sensing. Earlier, Zeng *et. al.* prepared a very light - reduced graphene oxide (rGO)/PDMS composite that resulted a wide linear sensing range (up to 110%), and has achieved a GF of 7.2.[29] Boland *et. al.* has showed an ultra-wide working strain of 800%, with a GF of 35, demonstrating a good cyclic stability in highly elastic natural rubber/graphene composites.[25] Nonetheless, the limiting durability due to cracking effects, and relatively lesser GF than CNTs are observed in case of graphene incorporation. Therefore, a synergistic approach involving the integration of CNTs with graphene has been employed to harness the effects of both 1D and 2D fillers. In the recent past, studies have shown the applicability of 3D filled PNCs for different applications. For example, Wang *et. al.* has shown that the dispersion of graphene oxide (GO)/ functionalized CNT (f-CNT) heterostructure hybrids within PDMS matrix display a 20-fold increase in thermal stability.[10] S. Roy *et. al.* has reported an increase in storage modulus of thermoplastic polyurethane (TPU) by 206% along with a significant increase in thermal stability by introducing multi-walled CNT (MWCNT)/ rGO hybrids.[9] Given its functionality, a detailed understanding of the structure- property relationship is essential.

When it comes to the matrix, TPU has been chosen for this work among various elastomers. TPU is a versatile polymer, with good affinity for carbon fillers.[23,31] It possess hard and soft segments with high molecular weight, containing rich chemical functionalities. Further, it exhibits excellent tensile strength, modulus which depends on the composition and backbone structure of polymer chains.[32] There exists a plenty of articles presenting TPU-carbon nanocomposites for various applications.[31–35] But, in the context of hybrid filler modification for strain sensing, there

exist very limited studies. From the scarce, a study by Liu *et. al.* has shown a tuneable strain-sensing behaviour in TPU through the addition of bifiller - CNT and graphene. The synergistic effect was shown to result in 7-fold increase in electrical conductivity.[36]

It is to be noted that the TPU is a polar matrix, and hence, the interfacial interaction between polymer chains and 3D fillers are more pronounced. This results in a hierarchically distributed structures which tend to form conductive networks. This hierarchical aggregate distribution, in other terms, their polydispersity is governed by the balance between the dual interfacial interactions[37] (i.e., inter-filler and matrix filler interactions). This stresses the importance of understanding filler morphologies in the light of interfacial interactions. In our previous studies, we have investigated such hierarchically distributed CNTs, and wrinkled graphitic nanofiller structures through X-ray scattering technique, alongside, considering the effect of matrix polarity.[38,39] The elucidation of such embedded morphologies within matrices requires a non-destructive, yet transmissive probing technique, which primarily is the small-angle X-ray scattering (SAXS).[40,41] The minimum and maximum length scale that could be probed by this technique relies on maximum and minimum resolvable scattering vector (q) by the measurement (for SAXS ~ $1 < D < 100$ nm), which are decided by the technical limitations. In order to elucidate larger structures, as in our case is the aggregates (few nanoparticle clusters), the limitation is overcome by ultra-small angle X-ray scattering (USAXS) technique (resolves ~ few hundred nm). This inverse space imaging technique has its own advantages over real-space imaging, where it has been shown to elucidate structure in multiple length scales.[41,42] Extensive structural elucidation in CB [43,44], CNT [45–47], and graphene [48,49] based PNCs were done using this technique, thereby establishing its applicability.

In this work, we investigate the enhancement effects in TPU, as a result of 3D nanofiller dispersion, considering the filler distribution, their structural confinement, and interfacial interactions. The enhancement in mechanical, electrical and electromechanical or strain sensing characteristics has been comprehensively analysed. Herein, we have utilised the synergistic few layers graphene (FLG), with f-MWCNTs as our 3D hybrid nanofillers, that are dispersed in TPU via solvent mediated filler distribution to yield thin, flexible, conductive films. The filler fractions being chosen are in such a way to examine the composites' behaviour - at, above, and below its percolation threshold. USAXS technique has been employed to explore aggregate morphologies of 3Ds', which are then complemented by other ex situ characterizations. A further deliberate structural elucidation is performed though an iterative model fitting of USAXS data. The electromechanical performance has been systematically investigated to explicate its applicability as a strain sensor, which resulted in both heightened, and stable sensitivity. This study provides a comprehensive understanding of structure-property relationship in 3D carbon-based elastomeric composites.

Materials

A commercially available aliphatic polyether based TPU known as Texin SUN-3006, an extrusion grade material with a hardness rating of 90 Shore A, a specific gravity of 1.08 g cm^{-3}, possessing characteristic molecular weight of approximately M_n = 79,000, M_w = 2,11,000, and melt flow index (MFI) of 5.1 g/ 10 min at 200 °C with a load of 2.16 kg. TPU was sourced from Covestro, India. The hybrid 3D carbonaceous nanofillers were synthesized in laboratory by immobilizing multi-walled carbon nanotubes (MWCNT–COOH) onto edge-functionalized few layers graphene (FLG-OH), whose details are mentioned elsewhere.[50] The organic solvent - N, N-

Dimethylformamide (anhydrous 99.8%) (DMF) was procured from Sigma Aldrich, while the other required chemicals were locally procured.

Preparation of TPU/3D composites

The elastomeric TPU composites were prepared via solvent mediated nanofiller dispersion through Doctor's blade method. Among the different casting techniques, a geometrically stable, well-defined thin film with uniform thicknesses were reported to be obtainable through this method.[51] In a typical solvent mediated technique, a solvent reduces polymer melt's viscosity improving the mobility of chains. This results due to the unfolding of polymer chains improving their dynamics that enhances the phase intrusions within them. Herein, a measured quantity of 3D nanofillers were subjected to extended sonication in an organic solvent (DMF) to produce a well-dispersed suspension. For the study, the nanofiller concentrations were chosen to be 10%, 15% and 20% of weight (wt%) of TPU (with ~12 wt% being the characteristic percolation threshold). On the other hand, a calculated amount of TPU (at 2 mg/ml) was dissolved in the same solvent at 90 ºC to produce a homogeneous solution. This optimised temperature was necessary to provide efficient gelation kinetics in the phase segregated TPU. The sonicated filler suspension was introduced into TPU solution, and vigorously stirred until homogeneity. The stirring continued under heat to evaporate the solvent to eventually achieve a viscous solution, which was then poured onto a pre-heated aluminium mould of dimensions 30 × 10 × 5 mm^3. Over the casting surface, a doctor's blade was swept to remove the excess gel, to obtain a uniform film. Further, multiple vacuum degassing steps were done to remove trapped air bubbles during the course of solvent evaporation. A thin, free standing, phase segregated film was then obtained through a thermoreversible gelation.

Characterization techniques

The analysis and characterization of the prepared films were performed through different techniques as follows: WAXD studies were conducted to observe the crystalline, and phase composition in neat as well as 3D incorporated PU composites using a lab source - Cu-Kα radiation with Panalytical Empyrean diffractometer. The data were collected for a range of 2θ between 10º to 65º at a step size of 0.05º. The micro morphological imaging was done using Axia Chemi scanning electron microscope by Thermo Scientific™, U.S. at an accelerating voltage of 30 kV. The surface features of as-prepared samples before and after the introduction of cyclic deformation were imaged. To observe internal conformation of filler aggregates, the cross-sectional SEM images were recorded in finely sectioned thin strips. The surface of the strips was precisely polished to evade topmost layer to expose internal conformities. The Raman spectra for neat as well as composite samples were recorded using Raman Spectrophotometer (RIMS-U-DC) using a 532 nm laser source, at a power of around 1mW. The spectra were recorded between 500 cm^{-1} to 3000 cm^{-1}. The temperature depended storage modulus of the films were measured using the device - DMA 850 by TA instruments™. The measurements were done for neat as well as composite TPU films under tensile mode in a dual screw clamping geometry. The temperature range was between 25 to 100 ºC, at a heating rate of 3 ºC/min. The modulus was measured at a constant frequency of 1 Hz, at an amplitude of 20 µm, with a preload force of 10^{-2} N.

The strain sensing behaviour of the prepared conductive composites were thoroughly investigated using an inhouse developed stretching device. The respective programmable device is capable of introducing a controlled, stepwise cyclic strain at desired strain rates. In this study, step-wise stretching, as well as repetitive stretch-relaxation cycles at different strain rates, with intermediate delay in each step was imparted on the samples. The conductivity measurements were performed using a Keithley source cum multimeter (model 2450), that recorded varying current as

a function of strain - under a constant applied voltage of 20V. The values of current were significantly lesser - between 10^{-5} to 10^{-4}A, so that the Joule's heating was considered to be negligible. Conductive leads for the measurements were created using a thin copper strip adhered on either ends of sample surface using silver paste.

The variation of electrical resistance as a function of applied strain was quantified using conventional parameter $\Delta R/R_0$ (where, $\Delta R = R-R_0$, with R being instantaneous resistance under strain, and R_0 is the resistance without strain). In order to examine the sensitivity of composite films, the dimensionless parameter – GF is calculated using the following equation

$$\mathbf{GF} = \frac{\Delta \mathbf{R}/\mathbf{R_0}}{\boldsymbol{\varepsilon}} \qquad \text{(i)}$$

Where, ε denotes the imparted strain given as $\Delta L/L_0$ (ΔL and L_0 being the change in length and original length respectively). GF apparently denotes the net variation in resistance upon a unit strain, signifying the sensitivity of a sensing element.

Ultra-small angle X-ray scattering (USAXS)

To investigate the structural configurations of 3D fillers within TPU, USAXS measurements were carried out at P03 beamline of PETRA III, DESY, Germany. The transmissive USAXS experiments were conducted at an X-ray energy of 11.8 keV corresponding to a wavelength of 1.044 Å, with sample to detector distance (SD) of 9550±1 mm. The incident X-ray beam, with a size of 23 × 27 μm^2 (horizontal x vertical) was scanned through 500 μm thick samples. The scattered X-rays from the sample were recorded using a PILATUS 2M detector (Dectris, Baden, Switzerland) with a pixel size of 172 μm. SD was chosen to be significantly large in order to resolve lower values of the scattering vector (q) that emphasizes relatively larges structures. The respective consideration was due to the fact that the composites were expected to possess

hierarchically agglomerated 3D filler within them.[37] The intensity varies with respect to scattering vector, q which is given as

$$\boldsymbol{q = \frac{4\pi}{\lambda}\sin(\theta)} \qquad \text{(ii)}$$

Where, λ is the wavelength of X-ray, and θ being half of the scattering angle.

USAXS images recorded from 2D detector were processed using the DPDAK software suite[52] to result in 1D scattering plots. These intensity (I) vs. q plots were obtained through azimuthal integration of pixel-wise intensity from the beam centre, which is referred as cake integration. The background subtraction and masking were done by following procedures explained in the literature.[53]

Scattering model

Elucidation of structural information from a standard scattering pattern could be performed through conventional model dependent, as well as model independent analysis. Recent developments in computing tools enable iterative model fitting of the obtained inverse-space scattering curves. Various scattering models incorporating the form, and structure factors along with the possibility of combining more than one structure factors, enables critical investigation of the scatterers. In this study, a simplified, and more generalized, shape independent *Guinier-Porod model* has been utilised to fit and analyse the scattering data. The Guinier-Porod model has been shown to determine various shapes including symmetric, asymmetric as well as intermediate structures. The Beaucage equation[40] that initially unified the Guinier and Porod regimes, was improvised for a smoother inter-regime transition by Hammouda[54]. The generalised function is given as

$$I(q) = \begin{cases} \frac{G}{q^s} exp\left(-\frac{q^2 R_g^2}{3-s}\right) & , q \leq q_1 \\ \frac{D}{q^m} & , q \geq q_1 \end{cases} \quad \text{(iii)}$$

Where, G and D are Guinier and Porod scaling parameters, R_g is the radius of gyration, q is the scattering vector, q_1 is the cross-over between Guinier and Porod regime, s is a shape dependent dimensionality parameter, and m is the Porod exponent. A more elaborate theoretical discussion on this model could be found elsewhere.[54]

For fitting the respective function to the experimentally obtained USAXS data, SasView software has been used. SasView is an open-source software package comprising a volume of scattering models for fitting the small angle scattering data. This inverse-space fitting tool undergoes iterative least square optimization on *I(q)* datasets for the selected model. Additionally, user-defined constraints could be assigned to ensure a physically reasonable estimates of the parameters. During fitting, the DREAM algorithm has been employed, and the fitting has been carried out for entire q range. The inclusive details of fitting are being discussed in the following section.

Results and Discussions

WAXD studies on the pristine TPU film, 3D fillers, and their composites depicting their crystalline and phase characteristics are shown in figure 1(a). A broad peak ranging between 13° to 30° centred at a 2θ of 20.03° for pure TPU, arises from the well-known planar reflection (110), depicting the typical interchain distance of 4.43 Å. In addition to the presence of soft and hard segments, which are of short-range order, the broadened peak suggests the presence of amorphous TPU moieties.[55] The intense (002) planar reflection from pristine 3D fillers at 2θ = 26.61° is a characteristic of interlayer spacing corresponding to 0.335 nm.[56,57] The two disrupted peaks at 42.42° and 44.58° attribute to (100) and (101) graphitic planes. Together with (002), relatively

feeble reflections from (004) planes at $2\theta = 54.71°$ are an indicative of the lamellar graphitic planes of FLG.[56] It is to be noted that the (002) peak positioned at 26.61° rather than 26.75° of graphite further suggests the presence of exfoliated C=C layers to result in the few layers. For the case of nanocomposites, a conventional increase in the intensity of (002), and (004) reflections corresponding to graphitic planes are observed with incremental filler loading. Contrarily, the intensity of (110) peak corresponding to TPU shows a decremental behaviour. This elucidates the fact that 3D fillers intrude within the interchain spacings of TPU, which is an indicative of increased interfacial interaction between 3D and TPU matrix.

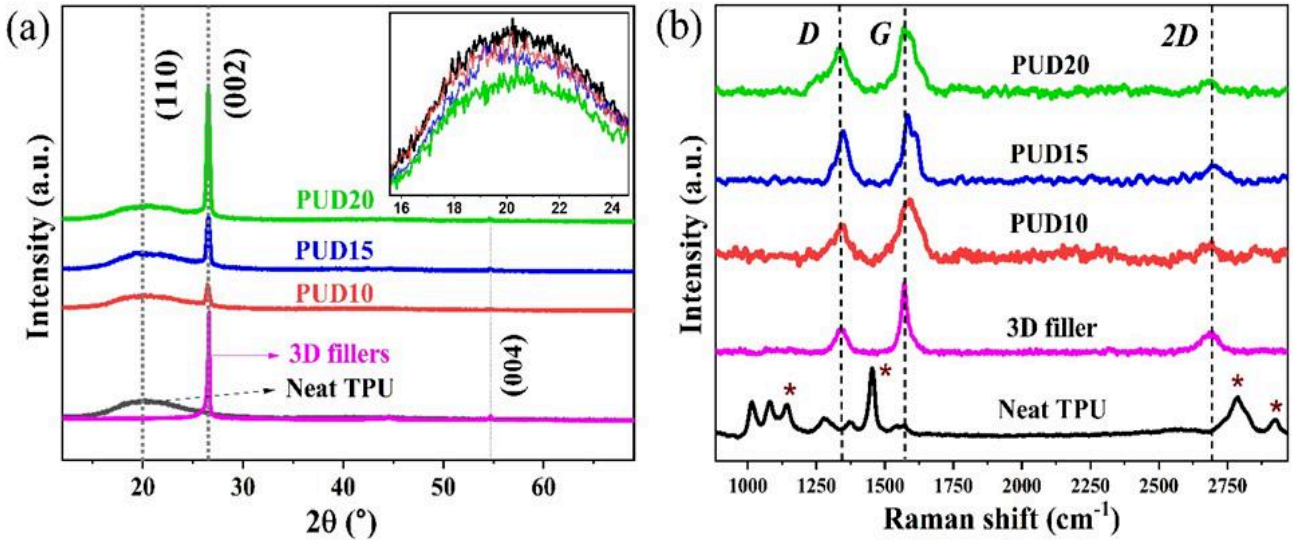

Figure 1. (a) WAXD patterns of neat TPU, 3D, and its composites shown with offset for comparison. Inset in a) shows the decrement of TPU's (110) peak intensity with filler concentration. (b) Raman spectrum of the samples with characteristic peaks of neat TPU; D, G and 2D peaks of 3D fillers being highlighted.

The Raman spectrum of TPU, 3D and their composites are shown in figure 1(b). From the spectra of 3D fillers, we evidence the characteristic D, G and 2D bands at 1340 cm^{-1}, 1570 cm^{-1}, and 2689 cm^{-1} respectively. The presence of 2D band is an indicative of FLG, arising due to the second-order overtone of in-plane transverse optical phonons from sp^2 hybridised carbon atoms, which is

sensitive to interlayer interactions, and stacking.[58] The G and D bands respectively are due to E_{2g} phonon mode that represents in-plane vibrational symmetry, and lattice disorders in sp^2 hybridized carbon structures. The spectra of neat TPU consisted the prominent peaks at 1445 cm^{-1}, corresponding to CH_2 bending; and two peaks at 2922 cm^{-1} and 2785 cm^{-1}, which are associated with CH_2 stretching; a peak at 1080 cm^{-1} corresponding to C-O-C stretching.[59] In case of composites, the characteristic D, G and 2D bands persisted, while the intensity of 2D band diminished. Similarly, the peaks corresponding to CH_2 bending (between 2700 and 2930 cm^{-1}), C-O-C stretching (at 1080 cm^{-1}) also exhibited a significant decrease in intensity. This results due to the reduced chain mobility in TPU moieties as a result of incremental 3D reinforcement.

Structural confirmation of 3D nanofillers

The macroscopic characteristics of elastomeric nanocomposites are greatly influenced by the nature of distribution and degree of agglomeration of nanofillers within polymer matrices. Henceforth, to explicate the structural confirmation of 3D nanofillers within TPU, we have performed SEM, as well as USAXS studies on the samples. In addition to as-prepared nanocomposites, we have imaged the same films after introduction of cyclic strain to understand the stress effects in their morphological features. From figures 2(a) to 2(c), the comparative SEM micrographs elucidating surface characteristic of as prepared, and strain introduced PUD15 films are shown. It has been observed that, upon introduction of a mechanical strain (20% shown in figure 2(b)), the surface of films gets wrinkled due to strain-localisation effect.[60] When the films were subjected to multiple stretch-contraction cycles at larger strain values (greater than 30%), we could observe multiple strain induced fracture sites. Few of such are shown in figure 2(c). These surface deformations usually occur for the strains above their elastic limit. Such disruptions result in irreversible sheet resistances during cyclic stretching.

Following the surface evaluation, the cross-sectional SEM imaging was performed to explore 3D structures. It is worth mentioning that, from both the cases viz. SEM and USAXS, the hierarchical conformation of 3D filler structures, in a polydisperse fashion within the matrices has been evidenced. This aspect has been widely discussed in carbon nanofiller systems, including our previous studies on CB, and CNTs within polymer matrices.[38,39] The representative hierarchical 3D filler structures within PUD20 samples are shown in Figures 2(d) to 2(f), in the order of aggregates, their distribution, and primary particles (a few particles cluster) respectively. In each case, no uniform or correlated size distribution is observed. In other terms, the distribution of nanofillers within TPU is polydisperse in nature. It is expected that such a distribution elevates the number of short contacts favouring overall electron transport.

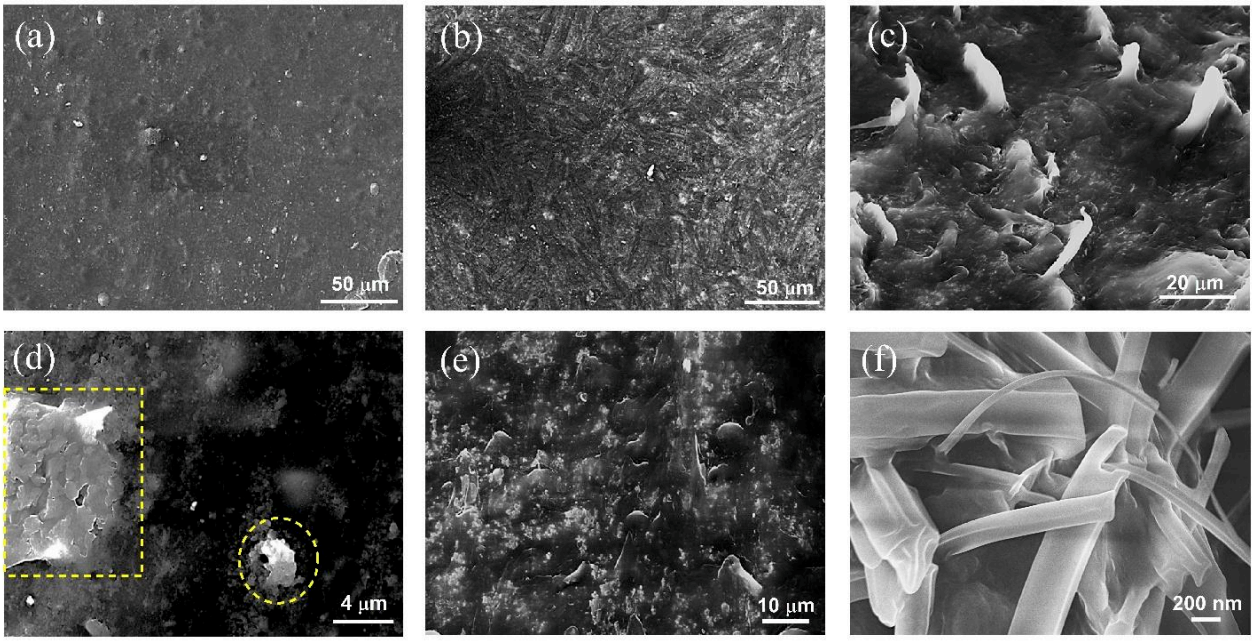

Figure 2. Representative SEM micrograph of as prepared PUD15 in (a), while (b) shows the same after introduction of 20% strain, and (c) the strain induced fractures on film surface above 30% of strain. The cross-sectional images of PUD20 sample shows polydisperse – (d) aggregates (highlighted), (e) dispersed aggregates, and (f) synergistic - 3D fillers within TPU matrices.

Inferences from USAXS model fitting

1D USAXS scattering plots of the TPU/3D composites are shown in figure 3. From the double logarithmic plots, one could observe that there are no characteristic peaks, which immediately infers the absence of strongly corelated or ordered structures in the system. To interpret structural conformities of 3D fillers, a simplified Guinier-Porod model has been fit to the obtained scattering data, which are shown in the figure 3. It is to be noted that the filler structures (including their agglomerates) are not confined into an explicitly definable geometry. Hence, a standard, shape independent model that could account for the non-symmetric structures is being considered for our case. One should note that the Guinier-Porod model does not account for indexing the polydispersity of scatterers. Hence, the degree of polydispersity is unquantifiable under present consideration.

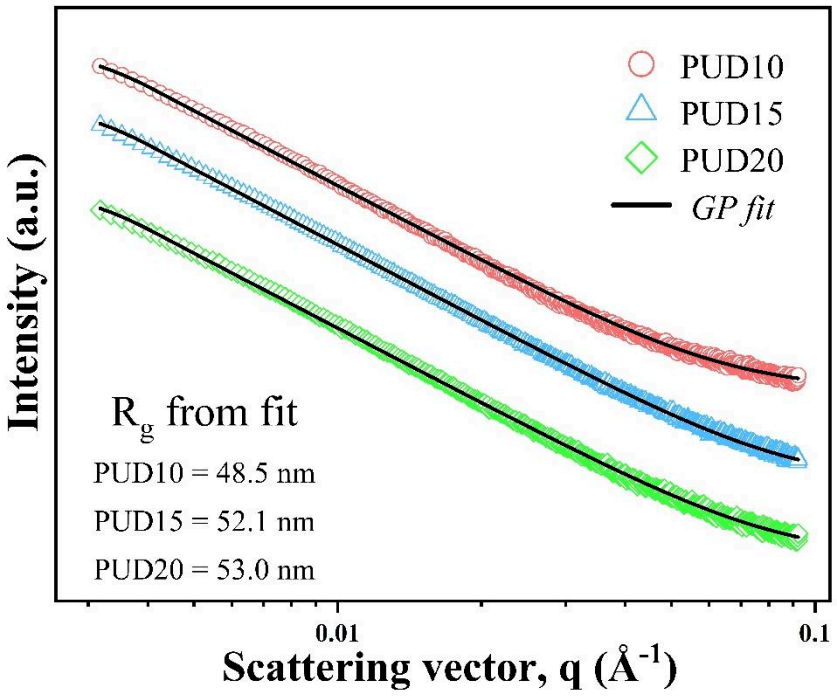

Figure 3. 1D scattering curves of TPU/3D composites along with the fitted data shown as solid line. The incremental R_g obtained from fitting are mentioned within the graph.

The structural parameters viz. R_g, s, and m that define size and shape has been obtained out of the best fits. In the present case, aggregate confirmations are the structures of interest, according to which, the constraints are defined for parameters. The obtained values along with fitting parameters are shown in table 1. One could observe that the minimum and maximum values of R_g are chosen in such a way that they correspond to the extrema of probed q values (with 0.0318 $nm^{-1} < q < 0.922$ nm^{-1}) guided by the equations: $D = 2\pi/q$ and $R_g = R(3/5)^{0.5}$. The equation corresponding to radii of globular spheres has been considered, since the preliminary fittings consistently yielded the value of s close to zero, for all composites.

Table 1. Parameters and fit values of USAXS model fitting. Note: The fits resulted negligible residuals distributed around the fitted values

*	s (-)	m (-)	R_g (nm)	D (nm)
Constraints (min and max)	*0 and 3*	*1 and 4*	*3 and 76*	*~ 7 and 197*
PUD10	0.02	2.94	48.5	125.3
PUD15	0.09	2.97	52.2	134.6
PUD20	0.03	2.95	53.0	136.8

From the obtained values, information on the nature of scatterers could be inferred comprehensively. To start with, we observe that the value of dimension-indicative parameter s is nearly zero for all the composites. From the theory of Guinier-Porod model, one could approximate that the aggregate conformities (on a global average) are globular structures.[54] Due to Van Der Waals forces between the fillers in vicinity, the aggregates inherently tend to confine symmetrically. Yet, the functionally rich TPU matrix tend to elicit its contribution to give rise to matrix-filler (or interfacial) interaction. It could be seen from SEM images that the clusters lacked

symmetrical morphologies. Hence, the resultant structures are a result of the balance between the said two interactions.

Contrary to the previously reported value of *m* between 3 and 4 for lamellar graphitic structures with surface fractals[61], and even lesser (1< m <2) for CNTs [62], the 3D structures display an intermediate behaviour. The obtained values of exponent (*m*) bridge between the mass and surface fractals, which depicts the structures to be branched, irregular networks.[54] Such branched structures of 3D aggregates could be accounted affirmative for the formation of transport networks within the TPU/3D composites. Moreover, the fit has yielded R_g values as ~ 48.5 nm, 52.2 nm and 53.0 nm corresponding to aggregate sizes (*D*) of 125.3 nm, 134.7 nm, and 136.9 nm for PUD10, PUD15 and PUD20 samples respectively. These values correspond to few nanoparticles' aggregate structures. It is understandable that the incremental filler loading results in large clusters due to pronounced filler-filler interaction than matrix filler interaction. From the electrical transport studies, we have observed that the percolation threshold is just above 10wt%; Concurrently, we see that, there is a relatively significant increase in average aggregate size just above percolation threshold - i.e. between 10 and 15wt% than the increment in between 15 and 20wt%. And, the subsequent addition of nanofillers may result in a relatively decreased rate of aggregation in matrices. This accounts to the fact that - just before percolation, the fillers span the matric, and a feeble loading above percolation onsets the bridging of interfacial transition zones between isolated clusters and primary particles.[6] This typical transition in morphology at percolation has been previously observed in carbon black aggregates[63,64]. It is affirmative to observe the respective behaviour in a dimensionally distinct 3D nanocomposite system as well, since, this suggests that 3D fillers also obey the similar percolative behaviour as that of other carbon fillers in polymer matrices.

Mechanical characteristics

DMA analysis has been carried out to understand the interfacial interactions between 3D filler and TPU matrix. In our previous study[38,39], we have observed the effect of one- and two-dimensional carbon fillers viz. MWCNT and graphene addition in polar and non-polar matrices. It has been observed that the intermolecular interactions between the moieties are critically affected by temperature, which alter the polymer chain dynamics. It has also been reported that the carbon filler infusion within matrices, not only affects the mechanical characteristics, yet it amends the critical temperature (such as glass transition) of composites.[65] Here, we have studied the (tensile) moduli of samples in a functional temperature range of typical strain sensors, which is between room temperature (RT ~26^{o}C) to 100^{o}C.

From the plot shown in figure 4, one could clearly evidence a consistent surge in storage modulus of TPU, with the addition of nanofillers. The room temperature storage modulus of the samples has been observed to be ~34.7, 54.2, 91.1 and 160.7 MPa for neat TPU, PUD10, PUD15 and PUD20 samples, respectively. Clearly, an increment of 56% in modulus with 10wt% nanofiller addition has been observed. While a significant surge of 163% and 363% was observed for 15 and 20wt% loading, respectively. This surge in modulus suggests the effect of 3D reinforcement within polymer moieties, resulting in a diverse mechanical behaviour of the nanocomposite. TPU being functionally rich, shows a higher degree of interfacial interaction with 3D carbon interfaces. The intrusion of 3D filler intervenes the dynamics of TPU polymer chains to result in an increased rigidity of composites. It is seen from the plot that, the modulus decreases with increase in temperature, which is attributed to an increased chain mobility. The predominant matrix-filler

interaction, hence suppresses with the emergence of active polymer chains - onset by an externally applied temperature.

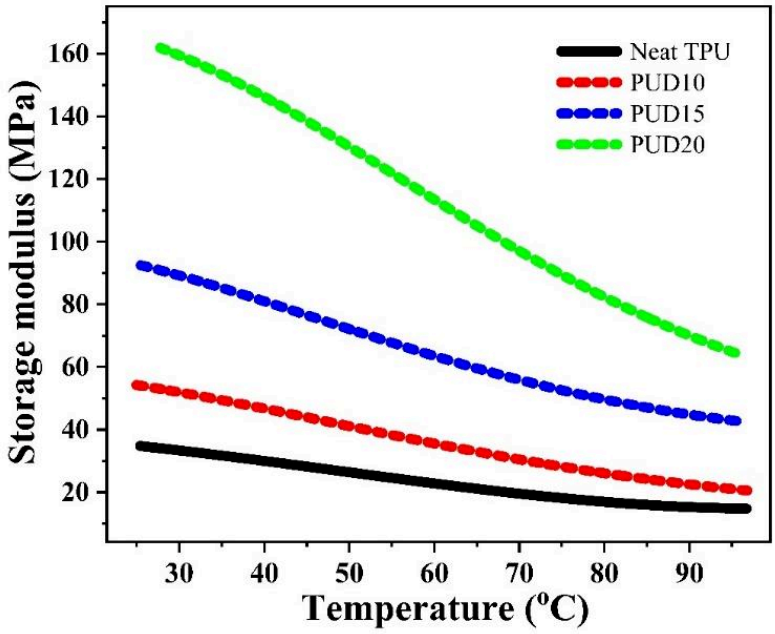

Figure 4. The temperature vs. storage modulus curves for neat as well as 3D incorporated TPU at different loading fractions, indicating a systematic increase in modulus with filler loading

From the degree of linearity in modulus versus temperature curves, one could understand the stability of filler networks within composites. A typical non-linear fall with temperature is observed at higher filler loadings, which is attributed to the breakdown of filler networks within elastomers.[66] Henceforth, we could infer from data that the 3D networks are significantly stable with temperature within TPU matrices which is beneficial for applications. To achieve enhanced electrical conductivity, the infusion of larger amount of nanofillers shall befit, but at the cost of reduced flexibility of the composites.

Electromechanical characteristics

The electromechanical studies, which depict stain-sensing capabilities of the prepared conductive films, has been systematically investigated under a controlled unidirectional, as well as cyclic strain. From the measurements, it was observed that PUD10 composite does not show a

considerable electrical conductivity, which is because of the filler loading lesser than its electrical percolation threshold. On the other hand, an enhanced conductivity, with an excellent strain response is observed for PUD15 and PUD20 composites. This shows that, TPU/3D composites produced through the simple solution casting possess a percolation threshold between 10 and 15wt%.

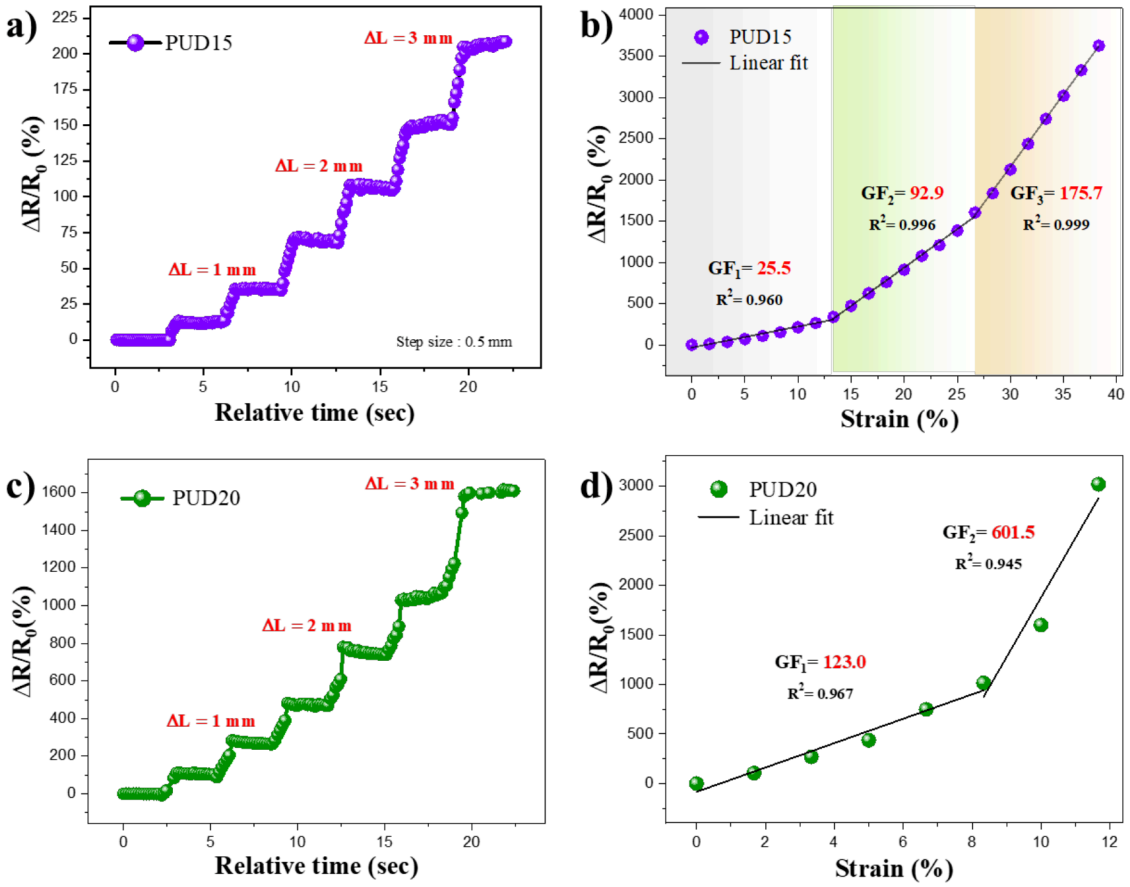

Figure 5. a) and c) shows the strain-dependent resistance change in PUD15 and PUD20 films respectively, under a constant step-wise strain, with a relaxation at each step to show their sensing stability. b) and d) illustrate strain vs $\Delta R/R_0$ plots of PUD15 and PUD20 respectively, which are fitted linearly to obtain GF in different stages of strain. The R^2 mentioned within the graphs indicate the co-efficient of determination depicting the goodness of fit.

The obtained strain-conductivity results are shown in figure 5. The stability of sensing has been tested by applying a uniform, step-wise strain up to 10% of its nominal length. An incremental

strain in steps of 0.5 mm, at a strain rate of 0.5 mm/sec, with a relaxation time of 2.5 seconds in each step has been applied and the respective electrical response are recorded. The obtained results are shown in figure 5(a) and 5(c). Both the films displayed an excellent response upon loading, with an appreciable stability in each step. It is clearly evident from the results that the relative resistance change ($\Delta R/R_0$) is significantly higher for PUD20 composite compared to PUD15. This is attributed to the higher concentration of 3D in PUD20, which facilitates the formation of a greater number of conductive network pathways. Furthermore, while imparting strain, there occurs a proportionally greater number of network breakdown, which reflects in the form of decreased electrical conductivity.

In order to determine the extent of linearity in sensing, the $\Delta R/R_0$ with incremental strain up to elongation at break has been recorded. The results are shown in figures 5(b) and 5(d). To determine GF, a linear fit was applied on the corresponding data, as indicated by solid lines in the plots. A linear GF (denoted as GF_1) of 25.5 has been observed for PUD15 composites, while PUD20 has resulted in a very high value of 123. This shows that the higher concentration provides a greater sensitivity; however, the extent of linear sensing is limited. In case of PUD20, the linear range is observed up to 8% strain, while it is 13% for PUD15. This limitation with higher concentration is because of the increased mechanical rigidity with loading which has been evidenced from DMA studies. Under large strains, in addition to conductive network breakdown, irreversible microscopic fractures arise in matrix, which further inhibits the transport efficiency. These fractures are also observed from SEM images shown in figure 2c. This typical trade-off between flexibility and sensing efficiency pertains in PNC systems. With a further increase in strain, the degree of increase in resistance steeps (regions: GF_2 in PUD20, and GF_3 in PUD15), resulting due to the intensification of network breakdown. In such higher strains, the prepared films have

displayed a GF of 175.7 for PUD15, and 601.5 for PUD20, respectively. It is to be noted that the PUD15 film have shown three regimes of linearity with incremental GF up on strain. This characteristic response in elastomeric films is exclusively governed by their mechanical property.

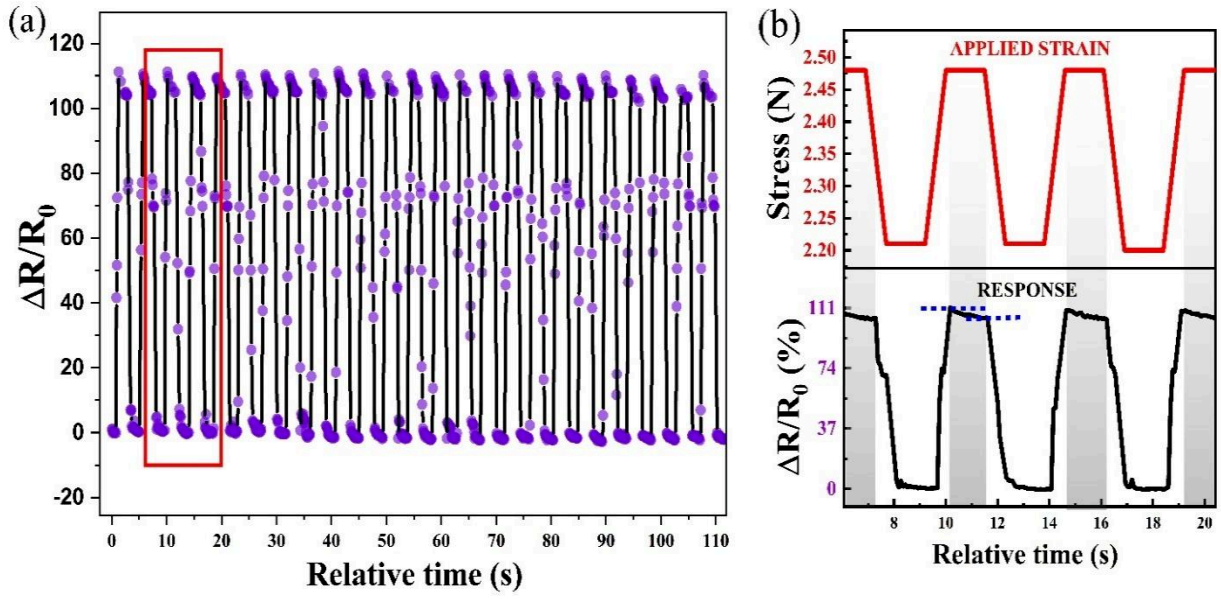

Figure 6. a) Cyclic strain sensing behaviour of PUD15 composite between 0% and 6.6% strain, showing its sheer stability within linear regime. b) Simultanoues plots of applied stress and its corresponding electrical response for a respresentative enlarged section of a). Blue lines indicated in b) shows the recovery of conductivity during delay time.

From the aforementioned studies on unidirectional strain, an optimal balance between flexibility and broad working (linear) range has been observed for PUD15 composite, while, an elevated small strain sensitivity has resulted in PUD20. Hence, PUD15 composite has been chosen to examine the cyclic stability under multiple stretch-compression cycles. The cycles were between 0% and 6.6% strain (ΔL between 0 and 2 mm), imparted at a strain rate of 2.5 mm/s, with a time delay of 1.5 seconds between the steps. The results have shown a consistent cyclic variation in resistance, which is illustrated in figure 6(a). An enlarged section of figure 6(a) is plotted simultaneously with the applied stress in figure 6(b), that further validates the consistent response.

One could observe a decrease in resistance during the delay time (indicated with blue lines in figure 6(b)), that specifies the recovery of conductive networks. Such recovery is ascribed to the elastic nature of matrix, which tend to revert it to their original shape after deformation, thereby reorienting the filler structures to partially recover the disrupted networks.

Conclusions

The functionally rich TPU elastomer, incorporated with 3D hybrid fillers were comprehensively studied in terms of their structural, mechanical and strain sensing behaviours. The preliminary characterization on the solution cast - thin, flexible composites via WAXD, and Raman spectroscopy has confirmed a superior reinforcement of 3D fillers within TPU matrices. Similarly, the pronounced interfacial interaction was also confirmed through mechanical analysis, which revealed a surge in storage modulus by 4.6 times of the neat elastomer, attributing to the TPU-3D synergy. These observations have further validated TPU as a promising host for multi-dimensional carbon nanofillers. Through deliberate structural analyses, it has been shown that 3D filler confine in a polydisperse fashion within polar TPU matrix. Moreover, the fitted USAXS data has interpreted an incremental aggregate dimension with concentration, that possessed - branched, and highly irregular filler confirmations. This structural aspect is considered highly favourable for the formation of conductive transport networks within the composites. Meantime, such similar aspects account significantly for an increased mechanical modulus of the composites.

The prepared elastomers displayed an excellent strain sensing behaviour in both unidirectional and cyclic strain. Herein, a 4.8-fold increase in the linear (low-strain) GF was observed upon increasing 3D loading from 15wt% to 20wt%. However, a comparable surge in mechanical modulus (4.6 times) is also observed for the same increment in concentration, which has significantly limited the working (linear) strain range for 20wt% composite. A maximum GF of

601 was achieved for strain above 8% (high-strain) in 20wt% 3D loading. The resulting high GF corresponding to respective working strain infers that TPU/3D composites are highly sensitive, and are exclusively applicable for small strain monitoring. In essence, this study has demonstrated the synergistic carbon hybrids as a potential choice for the fabrication of high-performance strain sensors; meanwhile emphasizing the requirement for strategic engineering of fabrication techniques to produce advanced sensor technologies.

Conflict of interest

There are no conflicts to declare.

Acknowledgement

The authors acknowledge DESY (Hamburg, Germany), a member of the Helmholtz Association HGF, for the provision of experimental facilities. Parts of this research were carried out at the beamline P03 of PETRA III and we thank P03 beamline staffs for their support. Beamtime was allocated for the proposal with ID: 20221139. The financial support from the Department of Science and Technology (DST, Government of India) provided within the framework of the India@DESY collaboration is gratefully acknowledged. V.B. and S.K.V. are deeply grateful for the contribution provided by Dr. Debmalya Roy, DMSRDE, Kanpur and his role in nurturing this scientific work, and also, to Dr. Subash Mandal from DMSRDE, Kanpur and Prof. Sravendra Rana from UPES for their discussions and timely suggestions. V.B. and S.K.V. acknowledges DMSRDE, Kanpur for providing the financial support under the CARS project (TR/0569/CARS-135). Sincere gratitude to Dr. Dileep Kumar, and Mr. Sharanjeet Singh from UGC DAE-CSR, Indore for helping with SEM imaging. The support from central research facility of IIT, Delhi (CRF-IITD) for DMA analysis, and Central Instrumentation Centre (CIC) of R&D UPES, Dehradun for Raman spectroscopy, and GIXRD measurements are gratefully acknowledged.

References

(1) Li, L.; Han, L.; Hu, H.; Zhang, R. A review on polymers and their composites for flexible electronics. *Materials Advances* **2022**, *4* (3), 726–746. https://doi.org/10.1039/d2ma00940d.

(2) Cima, M. J. Next-generation wearable electronics. *Nature Biotechnology* **2014**, *32* (7), 642–643. https://doi.org/10.1038/nbt.2952.

(3) Mokhtar, S. M. A.; De Eulate, E. A.; Yamada, M.; Prow, T. W.; Evans, D. R. Conducting polymers in wearable devices. *Medical Devices & Sensors* **2020**, *4* (1). https://doi.org/10.1002/mds3.10160.

(4) Van Le, C.; Yoon, H. Advances in the use of conducting polymers for healthcare monitoring. *International Journal of Molecular Sciences* **2024**, *25* (3), 1564. https://doi.org/10.3390/ijms25031564.

(5) Han, S.; Li, Q.; Cui, Z.; Xiao, P.; Miao, Y.; Chen, L.; Li, Y. Non-destructive testing and structural health monitoring technologies for carbon fiber reinforced polymers: a review. *Nondestructive Testing and Evaluation* **2024**, *39* (4), 725–761. https://doi.org/10.1080/10589759.2024.2324149.

(6) Guo, J.; Zhou, B.; Yang, C.; Dai, Q.; Kong, L. Stretchable and Temperature-Sensitive polymer optical fibers for wearable health monitoring. *Advanced Functional Materials* **2019**, *29* (33). https://doi.org/10.1002/adfm.201902898.

(7) Weng, W.; Chen, P.; He, S.; Sun, X.; Peng, H. Smart Electronic textiles. *Angewandte Chemie International Edition* **2016**, *55* (21), 6140–6169. https://doi.org/10.1002/anie.201507333.

(8) Hu, J.; Meng, H.; Li, G.; Ibekwe, S. I. A review of stimuli-responsive polymers for smart textile applications. *Smart Materials and Structures* **2012**, *21* (5), 053001. https://doi.org/10.1088/0964-1726/21/5/053001.

(9) Roy, S.; Srivastava, S. K.; Pionteck, J.; Mittal, V. Mechanically and Thermally Enhanced Multiwalled Carbon Nanotube–Graphene Hybrid filled Thermoplastic Polyurethane Nanocomposites. *Macromolecular Materials and Engineering* **2014**, *300* (3), 346–357. https://doi.org/10.1002/mame.201400291.

(10) Wang, S.-S.; Feng, D.-Y.; Zhang, Z.-M.; Liu, X.; Ruan, K.-P.; Guo, Y.-Q.; Gu, J.-W. Highly Thermally Conductive Polydimethylsiloxane Composites with Controllable 3D GO@f-CNTs Networks via Self-sacrificing Template Method. *Chinese Journal of Polymer Science* **2024**, *42* (7), 897–906. https://doi.org/10.1007/s10118-024-3098-4.

(11) Mora, A.; Verma, P.; Kumar, S. Electrical conductivity of CNT/polymer composites: 3D printing, measurements and modeling. *Composites Part B Engineering* **2019**, *183*, 107600. https://doi.org/10.1016/j.compositesb.2019.107600.

(12) Park, M.; Kim, H.; Youngblood, J. P. Strain-dependent electrical resistance of multi-walled carbon nanotube/polymer composite films. *Nanotechnology* **2008**, *19* (5), 055705. https://doi.org/10.1088/0957-4484/19/05/055705.

(13) Ding, X.; Jia, R.; Gan, Z.; Du, Y.; Wang, D.; Xu, X. Tough and conductive polymer hydrogel based on double network for photo-curing 3D printing. *Materials Research Express* **2020**, *7* (5), 055304. https://doi.org/10.1088/2053-1591/ab8cfb.

(14) Crosby, A. J.; Lee, J. Polymer Nanocomposites: The "Nano" effect on mechanical properties. *Polymer Reviews* **2007**, *47* (2), 217–229. https://doi.org/10.1080/15583720701271278.

(15) Kwon, N. K.; Kim, H.; Han, I. K.; Shin, T. J.; Lee, H.-W.; Park, J.; Kim, S. Y. Enhanced mechanical properties of polymer nanocomposites using Dopamine-Modified polymers at nanoparticle surfaces in very low molecular weight polymers. *ACS Macro Letters* **2018**, *7* (8), 962–967. https://doi.org/10.1021/acsmacrolett.8b00475.

(16) Bertolini, M. C.; Ramoa, S. D. a. S.; Merlini, C.; Barra, G. M. O.; Soares, B. G.; Pegoretti, A. Hybrid composites based on thermoplastic polyurethane with a mixture of carbon nanotubes and carbon black modified with polypyrrole for electromagnetic shielding. *Frontiers in Materials* **2020**, *7*. https://doi.org/10.3389/fmats.2020.00174.

(17) Ma, J.; Zhan, M.; Wang, K. Ultralightweight Silver Nanowires Hybrid Polyimide Composite foams for High-Performance Electromagnetic Interference Shielding. *ACS Applied Materials & Interfaces* **2014**, *7* (1), 563–576. https://doi.org/10.1021/am5067095.

(18) Amrhar, R.; Singh, J.; Eesaee, M.; Carrière, P.; Saidi, A.; Nguyen-Tri, P. TablePolymeric Nanocomposites-based advanced coatings for antimicrobial and antiviral applications: A Comprehensive Overview. *Results in Surfaces and Interfaces* **2025**, 100497. https://doi.org/10.1016/j.rsurfi.2025.100497.

(19) Gong, H.; Zhang, K.; Dicko, C.; Bülow, L.; Ye, L. Ag–Polymer nanocomposites for capture, detection, and destruction of bacteria. *ACS Applied Nano Materials* **2019**, *2* (3), 1655–1663. https://doi.org/10.1021/acsanm.9b00112.

(20) Zhang, W.-G.; Li, L.; Yao, S.-W.; Zheng, G.-Q. Corrosion protection properties of lacquer coatings on steel modified by carbon black nanoparticles in NaCl solution. *Corrosion Science* **2006**, *49* (2), 654–661. https://doi.org/10.1016/j.corsci.2006.06.017.

(21) Hou, L.; Zhou, M.; Gu, Y.; Chen, Y. WPU/CB/GO nanocomposites: in situ polymerization preparation, thermal, and anticorrosion performance evaluation. *Journal of Applied Polymer Science* **2019**, *137* (21). https://doi.org/10.1002/app.48716.

(22) Islam, M. R.; Pias, S. M. N. S.; Alam, R. B.; Khondaker, S. I. Enhanced electrochemical performance of solution-processed single-wall carbon nanotube reinforced polyvinyl alcohol

nanocomposite synthesized via solution-cast method. *Nano Express* **2020**, *1* (3), 030013. https://doi.org/10.1088/2632-959x/abc050.

(23) Ryu, J.; Kim, J.; Oh, J.; Lim, S.; Sim, J. Y.; Jeon, J. S.; No, K.; Park, S.; Hong, S. Intrinsically stretchable multi-functional fiber with energy harvesting and strain sensing capability. *Nano Energy* **2018**, *55*, 348–353. https://doi.org/10.1016/j.nanoen.2018.10.071.

(24) Tayyab, M.; Zizhe, L.; Rauf, S.; Xu, Z.; Sagar, R. U. R.; Faiz, F.; Tayyab, Z.; Rehman, R. U.; Imran, M.; Waheed, A.; Javed, R.; Surulinathan, A.; Zafar, Z.; Fu, X.-Z.; Luo, J.-L. Advanced Fabrication Techniques for Polymer-Metal Nanocomposite Films: State-of-the-Art Innovations in Energy and Electronic Applications. *Chemical Science* **2024**. https://doi.org/10.1039/d4sc04600e.

(25) Boland, C. S.; Khan, U.; Backes, C.; O'Neill, A.; McCauley, J.; Duane, S.; Shanker, R.; Liu, Y.; Jurewicz, I.; Dalton, A. B.; Coleman, J. N. Sensitive, High-Strain, High-Rate bodily motion sensors based on Graphene–Rubber composites. *ACS Nano* **2014**, *8* (9), 8819–8830. https://doi.org/10.1021/nn503454h.

(26) Liehr, S.; Lenke, P.; Wendt, M.; Krebber, K.; Seeger, M.; Thiele, E.; Metschies, H.; Gebreselassie, B.; Munich, J. C. Polymer optical fiber sensors for distributed strain measurement and application in structural health monitoring. *IEEE Sensors Journal* **2009**, *9* (11), 1330–1338. https://doi.org/10.1109/jsen.2009.2018352.

(27) Wang, X.; Li, J.; Song, H.; Huang, H.; Gou, J. Highly Stretchable and Wearable Strain Sensor Based on Printable Carbon Nanotube Layers/Polydimethylsiloxane Composites with Adjustable Sensitivity. *ACS Applied Materials & Interfaces* **2018**, *10* (8), 7371–7380. https://doi.org/10.1021/acsami.7b17766.

(28) Hong, Z.; Zheng, Z.; Kong, L.; Zhao, L.; Liu, S.; Li, W.; Shi, J. Welded Carbon Nanotube–Graphene Hybrids with Tunable Strain Sensing Behavior for Wide-Range Bio-Signal Monitoring. *Polymers* **2024**, *16* (2), 238. https://doi.org/10.3390/polym16020238.

(29) Zeng, Z.; Shahabadi, S. I. S.; Che, B.; Zhang, Y.; Zhao, C.; Lu, X. Highly stretchable, sensitive strain sensors with a wide linear sensing region based on compressed anisotropic graphene foam/polymer nanocomposites. *Nanoscale* **2017**, *9* (44), 17396–17404. https://doi.org/10.1039/c7nr05106a.

(30) Lan, M.; Jia, X.; Tian, R.; Feng, L.; Shao, D.; Song, H. Advancing multifunctional thermal management with multistate graphene/CNTs conjugated hybrids. *Carbon* **2024**, *219*, 118850. https://doi.org/10.1016/j.carbon.2024.118850.

(31) Fan, Q.; Qin, Z.; Gao, S.; Wu, Y.; Pionteck, J.; Mäder, E.; Zhu, M. The use of a carbon nanotube layer on a polyurethane multifilament substrate for monitoring strains as large as 400%. *Carbon* **2012**, *50* (11), 4085–4092. https://doi.org/10.1016/j.carbon.2012.04.056.

(32) Kotal, M.; Srivastava, S. K. Structure–property relationship of polyurethane/modified magnesium aluminium layered double hydroxide nanocomposites. *International Journal of Plastics Technology* **2011**, *15* (S1), 61–68. https://doi.org/10.1007/s12588-011-9006-0.

(33) Paleo, A. J.; Martinez-Rubi, Y.; Krause, B.; Pötschke, P.; Jakubinek, M. B.; Ashrafi, B.; Kingston, C. Carbon Nanotube–Polyurethane composite sheets for flexible thermoelectric materials. *ACS Applied Nano Materials* **2023**, *6* (19), 17986–17995. https://doi.org/10.1021/acsanm.3c03247.

(34) Dong, M.; Li, Q.; Liu, H.; Liu, C.; Wujcik, E. K.; Shao, Q.; Ding, T.; Mai, X.; Shen, C.; Guo, Z. Thermoplastic polyurethane-carbon black nanocomposite coating: Fabrication and solid

particle erosion resistance. *Polymer* **2018**, *158*, 381–390. https://doi.org/10.1016/j.polymer.2018.11.003.

(35) Haji, M.; Haddadi-Asl, V.; Jouibari, I. S. Carbon nanotube/polyurethane nanocomposites with surface-modified nanostructures. *Iranian Polymer Journal* **2022**, *31* (10), 1173–1182. https://doi.org/10.1007/s13726-022-01066-4.

(36) Liu, H.; Gao, J.; Huang, W.; Dai, K.; Zheng, G.; Liu, C.; Shen, C.; Yan, X.; Guo, J.; Guo, Z. Electrically conductive strain sensing polyurethane nanocomposites with synergistic carbon nanotubes and graphene bifillers. *Nanoscale* **2016**, *8* (26), 12977–12989. https://doi.org/10.1039/c6nr02216b.

(37) Lin, Y.-C.; Chen, C.-Y.; Chen, H.-L.; Hashimoto, T.; Chen, S.-A.; Li, Y.-C. Hierarchical self-assembly of nanoparticles in polymer matrix and the nature of the interparticle interaction. *The Journal of Chemical Physics* **2015**, *142* (21). https://doi.org/10.1063/1.4921567.

(38) Roy, D.; B, V.; Vayalil, S. K.; Gupta, A.; Prasad, N. E.; Sochor, B.; Schwartzkopf, M.; Roth, S. V.; Kraus, T. In Situ Study of Structure Formation under Stress in Stretchable Conducting Nanocomposites. *The Journal of Physical Chemistry Letters* **2023**, *14* (25), 5834–5840. https://doi.org/10.1021/acs.jpclett.3c00929.

(39) Roy, D.; B, V.; Mandal, S.; Gupta, A.; Sochor, B.; Vayalil, S. K.; Kraus, T. Origin of dynamic network formation of 2D nanofillers in a flexible matrix. *Small Structures* **2025**. https://doi.org/10.1002/sstr.202400608.

(40) Beaucage, G.; Kammler, H. K.; Pratsinis, S. E. Particle size distributions from small-angle scattering using global scattering functions. *Journal of Applied Crystallography* **2004**, *37* (4), 523–535. https://doi.org/10.1107/s0021889804008969.

(41) Robbes, A.-S.; Jestin, J.; Meneau, F.; Dalmas, F.; Boué, F.; Cousin, F. In Situ SAXS and SANS Monitoring of Both Nanofillers and Polymer Chain Microstructure under Uniaxial Stretching in a Nanocomposite with a Controlled Anisotropic Structure. *Macromolecules* **2022**, *55* (15), 6876–6889. https://doi.org/10.1021/acs.macromol.2c00618.

(42) Tiihonen, L. V.; Weir, M. P.; Parnell, A. J.; Boothroyd, S. C.; Johnson, D. W.; Dalgliesh, R. M.; Bleuel, M.; Duif, C. P.; Bouwman, W. G.; Thompson, R. L.; Coleman, K. S.; Clarke, N.; Hamilton, W. A.; Washington, A. L.; Parnell, S. R. Revealing microscale bulk structure in polymer-carbon nanocomposites using spin-echo SANS. *Soft Matter* **2024**. https://doi.org/10.1039/d4sm00578c.

(43) Beaucage, G.; Rane, S.; Schaefer, D. W.; Long, G.; Fischer, D. Morphology of polyethylene-carbon black composites. *Journal of Polymer Science Part B Polymer Physics* **1999**, *37* (11), 1105–1119. https://doi.org/10.1002/(sici)1099-0488(19990601)37:11.

(44) Rieker, T. P.; Hindermann-Bischoff, M.; Ehrburger-Dolle, F. Small-Angle X-ray scattering study of the morphology of carbon black mass fractal aggregates in polymeric composites. *Langmuir* **2000**, *16* (13), 5588–5592. https://doi.org/10.1021/la991636a.

(45) Jiang, Q.; Zhang, Q.; Wu, X.; Wu, L.; Lin, J.-H. Exploring the Interfacial Phase and π–π Stacking in Aligned Carbon Nanotube/Polyimide Nanocomposites. *Nanomaterials* **2020**, *10* (6), 1158. https://doi.org/10.3390/nano10061158.

(46) Kobayashi, H.; Shioya, M.; Tanaka, T.; Irisawa, T. Synchrotron radiation small-angle X-ray scattering study on fracture process of carbon nanotube/poly(ethylene terephthalate) composite films. *Composites Science and Technology* **2007**, *67* (15–16), 3209–3218. https://doi.org/10.1016/j.compscitech.2007.04.005.

(47) Vainio, U.; Schnoor, T. I. W.; Koyiloth Vayalil, S.; Schulte, K.; Müller, M.; Lilleodden, E. T. Orientation Distribution of Vertically Aligned Multiwalled Carbon Nanotubes. Journal of Physical Chemistry C **2014**, *118* (18), 9507–9513. https://doi.org/10.1021/JP501060S.

(48) Chi, E.; Tang, Y.; Wang, Z. In situ SAXS and WAXD investigations of polyamide 66/Reduced graphene oxide nanocomposites during uniaxial deformation. *ACS Omega* **2021**, *6* (17), 11762–11771. https://doi.org/10.1021/acsomega.1c01365.

(49) Ferreira, W. H.; Dahmouche, K.; Andrade, C. T. Dispersion of reduced graphene oxide within thermoplastic starch/poly(lactic acid) blends investigated by small-angle X-ray scattering. *Carbohydrate Polymers* **2018**, *208*, 124–132. https://doi.org/10.1016/j.carbpol.2018.12.055.

(50) Mandal, S.; Roy, D.; Prasad, N. E.; Joshi, M. Interfacial interactions and properties of cellular structured polyurethane nanocomposite based on carbonaceous nano-fillers. *Journal of Applied Polymer Science* **2020**, *138* (2). https://doi.org/10.1002/app.49775.

(51) Söz, C. K.; Yilgör, E.; Yilgör, I. Influence of the coating method on the formation of superhydrophobic silicone–urea surfaces modified with fumed silica nanoparticles. *Progress in Organic Coatings* **2015**, *84*, 143–152. https://doi.org/10.1016/j.porgcoat.2015.03.015.

(52) Benecke, G.; Wagermaier, W.; Li, C.; Schwartzkopf, M.; Flucke, G.; Hoerth, R.; Zizak, I.; Burghammer, M.; Metwalli, E.; Müller-Buschbaum, P.; Trebbin, M.; Förster, S.; Paris, O.; Roth, S. V.; Fratzl, P. A customizable software for fast reduction and analysis of large X-ray scattering data sets: applications of the new DPDAK package to small-angle X-ray scattering and grazing-incidence small-angle X-ray scattering. *Journal of Applied Crystallography* **2014**, *47* (5), 1797–1803. https://doi.org/10.1107/s1600576714019773.

(53) Pauw, B. R.; Smith, A. J.; Snow, T.; Terrill, N. J.; Thünemann, A. F. The modular small-angle X-ray scattering data correction sequence. *Journal of Applied Crystallography* **2017**, *50* (6), 1800–1811. https://doi.org/10.1107/s1600576717015096.

(54) Hammouda, B. A new Guinier–Porod model. *Journal of Applied Crystallography* **2010**, *43* (4), 716–719. https://doi.org/10.1107/s0021889810015773.

(55) Gao, J.; Hu, M.; Dong, Y.; Li, R. K. Y. Graphite-Nanoplatelet-Decorated Polymer Nanofiber with Improved Thermal, Electrical, and Mechanical Properties. *ACS Applied Materials & Interfaces* **2013**, *5* (16), 7758–7764. https://doi.org/10.1021/am401420k.

(56) Kumar, M. K. P.; Nidhi, M.; Srivastava, C. Electrochemical exfoliation of graphite to produce graphene using tetrasodium pyrophosphate. *RSC Advances* **2015**, *5* (32), 24846–24852. https://doi.org/10.1039/c5ra01304f.

(57) Fikry, M.; Abbas, M.; Sayed, A.; Nouh, A.; Ibrahim, A.; Mansour, A. S. Using a novel graphene/carbon nanotubes composite for enhancement of the supercapacitor electrode capacitance. *Journal of Materials Science Materials in Electronics* **2022**, *33* (7), 3914–3924. https://doi.org/10.1007/s10854-021-07585-9.

(58) Machado, B. F.; Bacsa, R. R.; Rivera-Cárcamo, C.; Serp, P. Preparation of Few-Layer Graphene/Carbon nanotube hybrids using oxide spinel catalysts. *C – Journal of Carbon Research* **2019**, *5* (2), 28. https://doi.org/10.3390/c5020028.

(59) Mandal, S.; Roy, D.; Mukhopadhyay, K.; Dwivedi, M.; Joshi, M. Large-scale dispersion of the hierarchical (1D, 2D and 3D) carbonaceous nanofillers in thermoplastic polyurethane through supramolecular self-assembly and extrusion. *Composite Interfaces* **2023**, *31* (5), 559–582. https://doi.org/10.1080/09276440.2023.2269344.

(60) Ebata, Y.; Croll, A. B.; Crosby, A. J. Wrinkling and strain localizations in polymer thin films. *Soft Matter* **2012**, *8* (35), 9086. https://doi.org/10.1039/c2sm25859e.

(61) Weir, M. P.; Johnson, D. W.; Boothroyd, S. C.; Savage, R. C.; Thompson, R. L.; Parnell, S. R.; Parnell, A. J.; King, S. M.; Rogers, S. E.; Coleman, K. S.; Clarke, N. Extrinsic wrinkling and single exfoliated sheets of graphene oxide in polymer composites. *Chemistry of Materials* **2016**, *28* (6), 1698–1704. https://doi.org/10.1021/acs.chemmater.5b04502.

(62) Tiihonen, L. V.; Weir, M. P.; Parnell, A. J.; Boothroyd, S. C.; Johnson, D. W.; Dalgliesh, R. M.; Bleuel, M.; Duif, C. P.; Bouwman, W. G.; Thompson, R. L.; Coleman, K. S.; Clarke, N.; Hamilton, W. A.; Washington, A. L.; Parnell, S. R. Revealing microscale bulk structure in polymer-carbon nanocomposites using spin-echo SANS. *Soft Matter* **2024**. https://doi.org/10.1039/d4sm00578c.

(63) Kim, J. H.; Hong, J. S.; Ishigami, A.; Kurose, T.; Ito, H.; Ahn, K. H. Effect of Melt-Compounding Protocol on Self-Aggregation and percolation in a ternary composite. *Polymers* **2020**, *12* (12), 3041. https://doi.org/10.3390/polym12123041.

(64) Lin, J.; Zhao, Q.; Chen, H.; Li, M.; Yuan, L. A numerical study of ITZ percolation in polyphase concrete systems considering the synergetic effect of aggregate Shape- and Size-Diversities. *Materials* **2023**, *16* (6), 2515. https://doi.org/10.3390/ma16062515.

(65) Grady, B. P.; Paul, A.; Peters, J. E.; Ford, W. T. Glass Transition behavior of Single-Walled Carbon Nanotube−Polystyrene composites. *Macromolecules* **2009**, *42* (16), 6152–6158. https://doi.org/10.1021/ma900375g.

(66) Yang, L.; Huang, S.; Wu, F.; Zheng, S.; Yang, W.; Liu, Z.; Yang, M. New insights into the elasticity and multi-level relaxation of filler network with studies on the rheology of isotactic

polypropylene/carbon black nanocomposite. *RSC Advances* **2015**, *5* (81), 65874–65883. https://doi.org/10.1039/c5ra10516a.